15TH IEA HEAT PUMP CONFERENCE
MAY 26–29, 2026 | HOFBURG
VIENNA 2026
DECARBONISATION THROUGH INNOVATION

Study of a very high temperature heat pump (reverse Brayton cycle) for industrial decarbonization

Nicolas Tauveron[a], Robin Gautier[a], Pierre Dumoulin[a], Mathieu Menoux[a], Karthik Bhairapurada[b], Paul Burnier[b*]

[a]Univ. Grenoble Alpes, CEA/LITEN/DTCH, Grenoble, France
[b]Enogia, Marseille, France

Abstract

Industrial decarbonization requires high-temperature heat (above 400 °C), which is currently supplied mainly by the combustion of fuels such as oil, coal or natural gas. Although electrification offers a promising pathway toward decarbonization, its overall efficiency is often limited. As a result, industries are investigating alternative solutions tailored to their specific processes.
This paper presents work carried out on a very high-temperature heat pump concept capable of delivering temperatures up to 400 °C. A numerical study was performed on several case studies involving different strategies for recovering waste heat available at various temperature levels (20 to 150 °C). The study examines how the heat-pump architecture and the choice of working fluid influence performance across these scenarios. A prototype with a capacity of several tens of kilowatts, designed to reach such high output temperatures, is currently under construction. It has been developed to allow testing with different working fluids under the conditions corresponding to the studied case scenarios, enabling experimental validation of the challenges identified through numerical simulations. CFD simulations have also been carried out on this prototype, providing performance predictions for the complete heat-pump system as it will operate on the test bench.

Keywords: High temperature heat pump; Reverse Brayton cycle; Natural fluid, compressor technology; Carnot efficiency

1. Introduction

The decarbonization of heat and electricity production is paving the way for new technological solutions. In the industrial sector, heat is required across a wide range of temperatures, typically categorized as low-grade (below 150 °C), medium-grade (150–400 °C), and high-grade (above 400 °C). Low- and medium-grade heat account for more than half of the total industrial heat demand, which continues to rise [1]. At present, most of this demand is met by fossil fuel boilers, representing a major source of CO_2 emissions. Achieving carbon neutrality therefore calls for a fundamental transition toward cleaner heat supply technologies.

The conventional decarbonization solution involves using electric resistance heating elements. Due to limited efficiency, alternative solutions must be investigated, focusing on concepts that reduce energy consumption and improve the Levelized Cost of Heat (LCOH). Heat pumps have emerged as a promising alternative, as they can upgrade low-grade waste heat into useful thermal energy using electricity, without combustion. They also help balance electricity and thermal energy demand, enhancing grid stability—an increasingly important advantage in an electrified system reliant on renewable sources. However, current industrial heat pumps are largely limited to low-temperature applications below 100 °C due to fluid and technical constraints. Systems capable of delivering temperatures above 160 °C without additional mechanical vapor compression remain mostly at the prototype stage [2]. Recently, a Stirling cycle-based heat pump developed by Olvondo Technology managed to reach 200 °C [3]. Expanding the operational temperature range of heat pumps is a key research focus for enabling their replacement of fossil-fuel-based heating systems in industry.

* Corresponding author. Tel.: +33(0)4.38.78.61.51
E-mail address: nicolas.tauveron@cea.fr

Furthermore, the increasing penetration of intermittent electricity into grids necessitates considering energy storage. This energy will subsequently be used in the form of electricity or heat. Carnot batteries offer the advantage of storing energy as heat, allowing for its restitution in both energy vectors (electricity and heat); very high-temperature heat pumps (above 300 °C) can improve the charging efficiency of these storage systems. Indeed, different Carnot battery concept rely on very high-temperature heat pumps [4].

The present study aims to evaluate the potential of a reversed-Brayton heat pump cycle from both theoretical and experimental perspectives. A numerical study was first conducted on several case studies, involving different approaches for supplying thermal energy (waste heat) to the heat pump, various working fluids, and two distinct cycle architectures. Based on these results, a decision was made to design and build a dedicated test bench to experimentally assess the most promising configurations. A multi-kilowatt prototype capable of reaching high output temperatures is currently under construction. It was designed to accommodate various working fluids and different hot and cold source conditions, thereby enabling the experimental validation of the challenges identified in the numerical analysis. Computational Fluid Dynamics (CFD) simulations were performed to support the turbomachine design, providing predictions of the achievable performance on the test bench and contributing to the refinement of its final configuration.

Based on similar considerations, different international initiatives were launched to build experimental prototypes in order to study various experimental applications[5]. Furthermore, we mention that these works (including our) take benefit of historical or more recent efforts to develop very high temperature heat-pump for other applications (medium to high temperature compressors are under investigations in various Adiabatic Compressed Air Energy Storage (A-CAES) programs in CAES context [6], Helium High Temperature (HHV) (850°C) prototype in nuclear high temperature context [7]).

2. Configurations Studied

2.1. Focus on two specific technical contexts

In the present study, two specific techinical contexts are adressed: 1) high-grade heat pump for a direct use of thermal industry in heavy industries 2) high temperature heat pump as a part of a high temperature Carnot battery. Moreover, note that waste heat valorization is a key point to obtain higher Coefficient Of Performance (COP) and to ensure a better profitability of such system.

In addition, we mention that there could exist a specific case that involves the simultaneous production of both heat AND cooling by the heat pump. This is referred as a combined heat and cooling system, capable of providing both high-temperature heat and cooling for industrial processes. However, this application case is rare at such high heating temperatures, and we prefer to concentrate initially on more common scenarios.

2.2. Fluids to be Heated

At temperatures above 350°C, the fluids commonly used in industry and Carnot batteries are air and molten salts. Very few thermal oils are compatible with such a high temperature, and their cost is extremely high, which makes this application case very limited. Using steam as a heat transfer medium at very high temperatures faces major practical constraints. Above about 350 °C, the required pressure becomes extremely high (around 16 MPa), demanding heavy, expensive, and safety-critical equipment. Superheated steam can extend the usable temperature range without further increasing pressure, but it introduces other challenges such as reduced heat transfer coefficients, higher thermal losses, and increased material stress due to large temperature gradients. Consequently, despite its maturity and excellent thermophysical properties, steam is generally unsuitable for efficient and safe heat transfer in very high-temperature applications.

Some molten nitrate-based thermal fluids are suitable for high-temperature applications A minimum temperature is recommended to prevent these salts from solidifying, and a maximum temperature threshold must be respected to prevent their degradation. To target a broad application scope, we first focused on the most widespread salt, solar salt (a binary mixture of $NaNO_3$ and KNO_3), which has a recommended operating range of 280°C to 580°C [8]. An alternative salt is the HITEC XL (composed of $NaNO_3$–KNO_3–$NaNO_2$) which have a solidification temperature at about 120°C and a maximum acceptable temperature of 480°C [9].

2.3. Heat Sources Utilized

Utilizing industrial waste heat can substantially improve the performance of heat pumps and associated Carnot battery systems. By integrating waste heat as the low temperature source, the temperature lift is reduced, which directly increases the achievable COP of the heat pump. In turn, a higher COP improves the round-trip efficiency of a Carnot battery, since less electrical consumption is required to achieve a given output during charging and lower losses during discharging.
Moreover, for example, in the European Union, large shares of industrial waste heat are found in streams up to ~200 °C, and many heat sources fall into the 60-140 °C bracket for sectors such as chemicals, metals, food, pulp & paper etc [10]. This suggests that targeting this temperature band offers large potential: many processes already generate waste heat here, which could be upgraded (by heat pumps or heat upgrade technologies) to useful process temperatures, reducing fossil fuel heating.

2.4. Studied System Overview

The heat pump system under investigation is shown in Figure 1. Its purpose is to heat air from 20 °C up to 430 °C. This value was chosen in order to potentially heat molten salt, although the fluid has not been tested in the present study. It can be supplied by industrial waste heat, with a temperature $T_{waste} \in [20;\ 150\ °C]$. This waste heat can be delivered to the system either upstream of the hot heat exchanger (HHX) and/or upstream of the cold heat exchanger (CHX). Both configurations are investigated in this paper. In addition, a "manufacturer-oriented" approach is adopted, in which the thermal power of the heat pump is fixed at 1MW. This power corresponds only to the heat transfer ocurring in the HHX, **meaning that 1MW are dedicated to heat the air** from T_{waste} up to 430 °C.

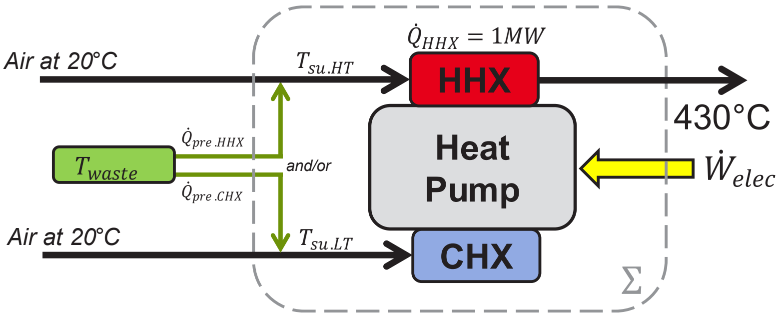

Figure 1: Heat pump system considered.

3. Numerical study

3.1. Fluid first restriction

Different families of fluids are theoretically usable. The gases traditionally studied in the literature are Helium, Argon, Nitrogen, and Air. While supercritical CO_2 is attractive for power Brayton cycles due to its high density and compact turbomachinery near the critical point, it becomes impractical for a reverse-Brayton heat pump targeting 350–400 °C. At these temperatures, CO_2 operates far above its critical point, requiring very high pressures (typically 10–25 MPa) to achieve sufficient working density. Such pressures impose severe constraints on materials, sealing systems, and safety measures, increasing CAPEX and operational complexity. Moreover, the thermodynamic advantages of near-critical CO_2 vanish at these elevated temperatures, and its strongly pressure-dependent properties complicate turbomachinery and heat-exchanger design, ultimately reducing achievable system COP when accounting for auxiliary losses and leakage. In contrast, single-phase gases such as air, nitrogen, argon, or helium offer predictable thermodynamic behaviour across this temperature range, allow much lower operating pressures, and rely on mature, industrially proven turbomachinery and heat-exchanger technology. These gases thus provide a safer, more economical, and technically robust solution for high-temperature reverse-Brayton heat pumping, making CO_2 an unsuitable choice for our applications.

Although water/steam is widely used in conventional high-temperature heat transfer and power cycles, it is unsuitable as a working fluid for a reverse-Brayton heat pump delivering 350–400 °C. To operate as a high-temperature heat pump, water would need to remain in a single-phase vapor throughout the compression and expansion stages. Achieving this at 350–400 °C requires extremely high pressures (~16–25 MPa or more, depending on superheat), which introduces severe material, sealing, and safety constraints. Moreover, steam's strong temperature-dependent specific volume and latent heat behaviour complicate turbomachinery and regenerator design, and any condensation would be catastrophic for system operation. Unlike air, nitrogen, argon, or helium, water cannot remain single-phase across the entire cycle at these temperatures without entering the supercritical region, which brings additional complexity and cost. In contrast, inert gases and air provide predictable single-phase behaviour, operate at much lower pressures, and allow the use of mature turbomachinery and heat exchangers. For these reasons, steam/water is considered impractical for a 350–400 °C reverse-Brayton heat pump, compared to gases such as air, N_2, Ar, or He.

To be fair, more sophisticated configurations could be envisioned, such as using multi-component gas mixtures or employing cascade cycles where CO_2 or steam cycles might appear in intermediate stages. Such approaches could, in principle, offer improved performance or take advantage of specific fluid properties. However, for the present study, we deliberately limit ourselves to simpler, single-phase gases (air, N_2, Ar, He) to reduce technical complexity, maintain manageable pressures, and rely on mature, proven turbomachinery and heat-exchanger technology. This approach ensures a robust and practical foundation before considering more complex configurations.

3.2. Architecture considered and Typical Application Cases

The reversed-Brayton architecture of the heat pump, considered in this study, is presented in Figure 2. The working fluid, at low pressure and low temperature, is first preheated in the CHX. It is then further heated by passing through the internal heat exchanger (IHX), depending on the configuration. Subsequently, its pressure and temperature are increased in the compressor before transferring its heat in the HHX. The fluid temperature can then be further decreased in the IHX, if this component is used. Finally, the fluid expands in the turbine, where its pressure and temperature are reduced to the initial conditions of the cycle. Note that the turbine and compressor are installed on the same shaft; therefore, the mechanical work produced by the turbine reduces the work required from the motor to drive the compressor.

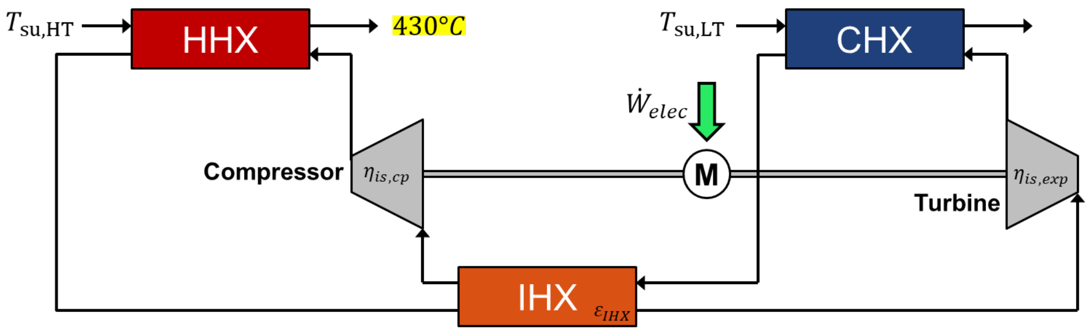

Figure 2: Diagram of the reversed Brayton Heat Pump.

Three configurations are considered, differing by where the waste heat is utilized: at the HHX inlet (case 1), at the CHX inlet (case 2) or at both inlets (case 3). Each configuration is studied with or without an IHX. In these cases, the use of waste heat allows the fluid to be preheated from T_{air} to T_{waste} before entering the heat exchanger. The method used to achieve this is beyond the scope of this study.

Table 1: Temperature at the inlet of the two external heat exchangers according to the configuration.

Configuration	C1	C2	C3
$\boldsymbol{T_{su,LT}}$	T_{air}	T_{waste}	T_{waste}
$\boldsymbol{T_{su,HT}}$	T_{waste}	T_{air}	T_{waste}

3.3. Numerical model

The cycle is modeled in *Python* and is based on the real-gas assumption. The thermodynamic library REFPROP is used **[11]**, together with its wrapper *REFPROPdll* , to compute the thermophysical properties of the working fluid throughout the cycle. The pinch-point methodology is applied to the external heat exchangers, with selected values of 30 °C for both the HHX and CHX. For the HHX, the pinch point is applied on both sides. This approximation is considered appropriate due to the similar temperature levels and the counter-current configuration of the heat exchangers. The IHX is modeled with a fixed thermal effectiveness of 80% when included in the cycle, and 0% otherwise. Finally, the isentropic efficiencies of the turbomachinery are set to 70% and 60% for the compressor and the turbine, respectively. Moreover, all type of losses: (electromechanical, pressure drops, heat losses, etc.) are all neglected is this study.

Usually, the interest value to assess the performances of a heat pump is the COP, defined as:

$$COP_{HP} = \frac{\dot{Q}_{HHX}}{\dot{W}_{compressor} - \dot{W}_{turbine}} \qquad (1)$$

With $\dot{Q}_{HHX}$ the thermal power exchanged in the HHX (fixed at 1MW), $\dot{W}_{compressor}$ the mechanical power provided to the compressor and $\dot{W}_{turbine}$ the mechanical power produced by the turbine. Note that considering the “manufacturer approach” (section 2.4), for an identical COP, the mass flow rate delivered by the heat pump varies depending on the temperature lift $(430 - T_{waste})$.

3.4. Impact of the Fluid

The four single-phase gases introduced in section 3.1 are first compared in Figure 3), using the configuration C1 and with an IHX. Overall, the COP is very similar for these four gases, regardless the waste-heat temperature level. However, the compression ratio required by the air and nitrogen is significantly higher than the one require by the argon and helium while the volumetric flow rate at the compressor inlet is about 50% higher for the first group of gases. This would strongly affect the design and feasibility of the turbomachinery and heat exchangers. Moreover, Helium, due to its very small molecules, requires higher sealing performance, which is difficult to guarantee for large components (exchangers, compressors...) [7].

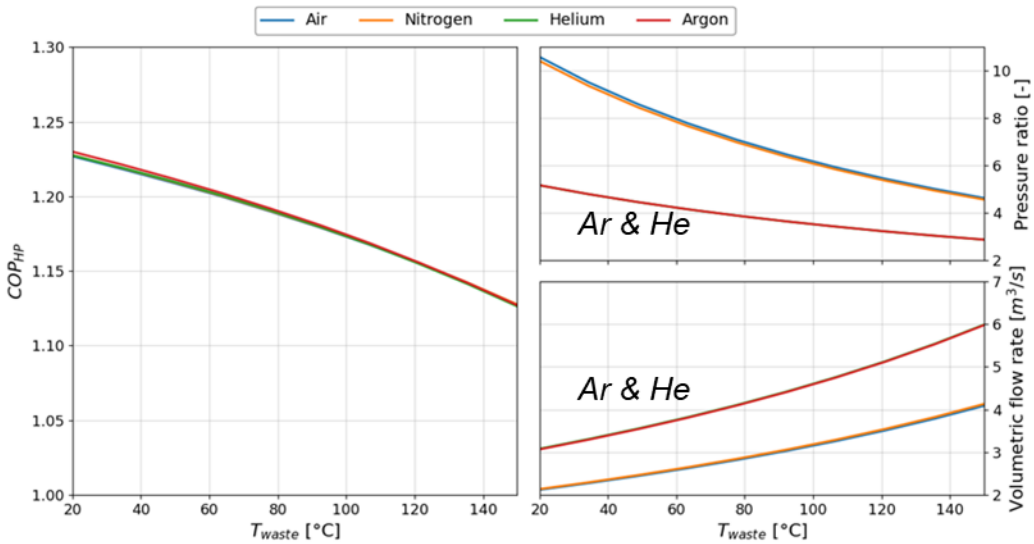

Figure 3: COP, pressure ratio and volumetric flow rate at the compressor inlet for the 4 tested gases working in the configuration C1 with an IHX.

3.5. Impact of Architecture

The numerical analysis focuses on the different configurations and architectures considered, using air as the working fluid since it is abundant, inexpensive, and easy to handle. Figure 4(a) shows the heat pump COP for the three different configurations versus waste-heat temperature level. The supply of waste-heat at the HHX

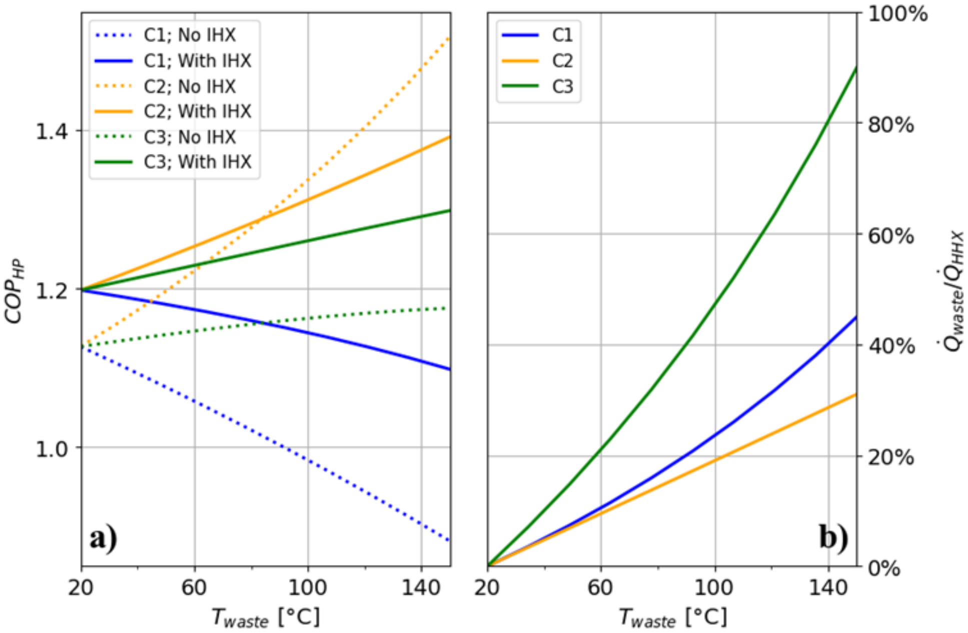

Figure 4: **a**) COP_{HP} of the 3 configurations with and without IHX. **b**) Amount of waste heat power used with the 3 configurations with IHX. Working fluid: air.

inlet (configuration C1) is detrimental to the COP. On the other hand, the supply of waste-heat at the CHX outlet (C2) improves the COP. Note that for this configuration, when T_{waste} > 80 °C, the usage of an IHX actually worsen the COP, as temperatures at the low-pressure side become higher than at the high-pressure side, reverting the heat flow. Providing waste-heat both at HHX inlet and CHX outlet (C3) does not improve the COP further. Moreover, Figure 4(b) shows that the required waste-heat rate is also favourable in C2, as it requires less waste-heat power than in C1.

3.6. Discussion on the COP definition

The COP definition introduced in Eq. (1) is valid only for the heat pump itself. However, when waste heat is considered, this definition can be extended to the whole system, as illustrated in Figure 1. Indeed, it is more appropriate to include the waste-heat used to preheat the air before its entrance into the HHX in the power term of the COP's definition, since it is part of the overall heat valorization process.

$$COP_{\Sigma} = \frac{\dot{Q}_{heating\ 20\rightarrow 430°C}}{\dot{W}_{compressor}-\dot{W}_{turbine}} = \frac{\dot{Q}_{pre,HHX}+\dot{Q}_{HHX}}{\dot{W}_{compressor}-\dot{W}_{turbine}} \qquad (2)$$

The system COP is plotted as a function of the waste-heat temperature in Figure 5. Configuration C3 outperforms the other two; however, its requirement for waste-heat power is significantly higher, as observed in Figure 4(b). These results differ significantly from Figure 4(a). Hence, only studying the heat pump COP is insufficient for establishing waste-heat valorization scenarios. The power recovered from the waste-heat and its limited quantity also need to be considered.

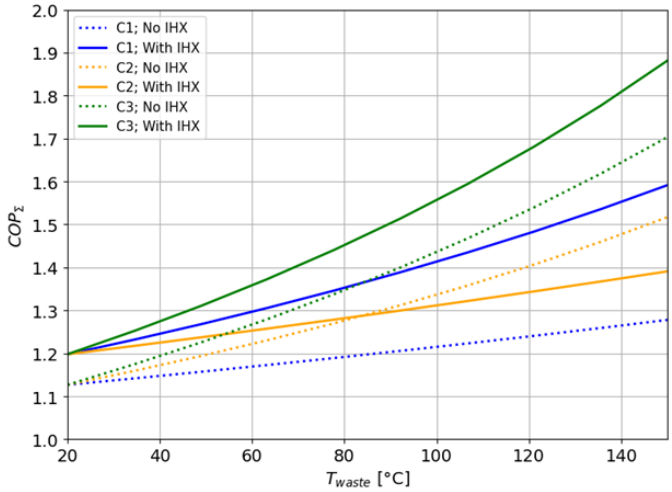

Figure 5: COP_{Σ} for the 3 configurations considered (air)

4. Experimental Validation Phase

4.1. Prototype parameters

To reinforce the findings of the numerical study, an experimental test bench has been developed. Its main purpose is to measure the actual COP of the system and to compare the various configurations and architectures presented in section 3. Given the high cost of a 1 MW prototype, a smaller heat pump with a capacity of 30–40 kW has been designed and is currently under construction. It will be running in closed loop with air, nitrogen or argon at a mass flow rate of 0.1 to 0.2 kg/s, depending on the gaz. The high temperature target of 430 °C remains the same. Therefore, the compressor will have to heat-up the working fluid up to more than 450 °C with a pressure ratio of 5 with air. Thus, the design of turbomachinery is the most critical part of the development of this heat pump prototype (see next section).

The prototype will be installed on a bench test which is able to supply air at the specified mass flow (from 0 to 0.1 kg/s) and temperature (between 20 and 150 °C) at the inlets of both external exchangers (HHX and CHX). This setup allows the simulation of waste heat at different temperature levels for the three proposed configurations of table 1. Several use cases have been defined including the one presented in Figure 6.

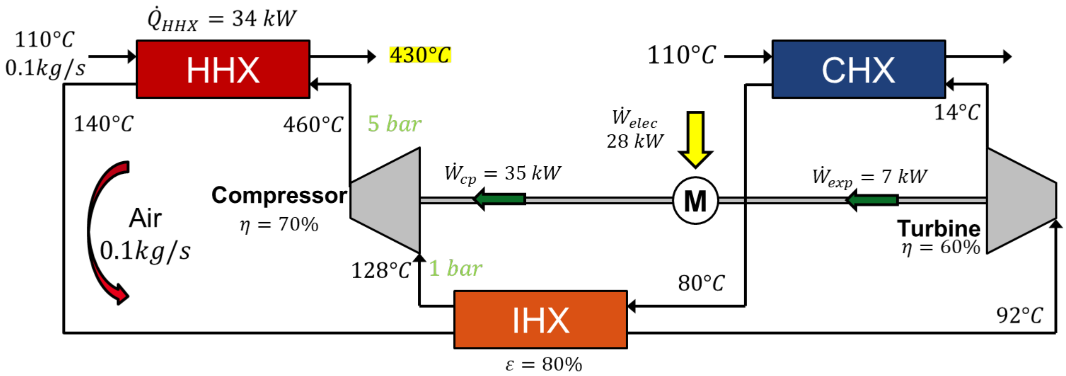

Figure 6: Experimental heat pump diagram showing the predicted numerical values for one of the defined use cases.

4.2. Turbomachinery Sizing Calculation

The compressor and turbine were defined to ensure optimal performance across a wide range of operating points compatible with the various use cases and working fluids. Both have been design and manufactured by the French company Enogia **[12]**.

4.2.1. Compressor design

The reference point retained for the compressor is as follows:
- Fluid: Air at 0.1kg/s
- Inlet: 1bar, 128°C

To accommodate variations in inlet temperature, pressure, and working fluid properties and to enable partial-load operation by bypassing selected stages, the compressor system was configured as two two-stage centrifugal compressors arranged in series. Each two-stage compressor is driven by a 30 kW permanent magnet synchronous motor (PMSM) rated at 55,000 rpm. The motors are controlled by a variable frequency drive (VFD), allowing variable-speed operation for performance optimization under different operating conditions.

The aerothermal design of the first operating point was carried out based on a preliminary design derived from the Cordier diagram, assuming a nominal rotational speed of 50,000 rpm and a design mass flow rate of 0.1 kg/s. The pressure-rise coefficient (ψ) was estimated using the empirical correlations proposed by Casey (Eq. 9.17) [13], which provided the corresponding stage flow coefficient (φ) for the preliminary sizing of the impeller and the vaneless diffuser according to Aungier's methodology [14]. Table 2 summarizes the key design parameters for each stage, including the stage flow coefficient, pressure-rise coefficient, and thermodynamic conditions.

To minimize conductive heat transfer from the compressor volutes to the motors, ceramic-based thermal shields were installed on both sides of each motor housing. This arrangement effectively reduced the heat conducted from the high-temperature compressor regions. Furthermore, to limit the area exposed to hot gases, vaneless diffusers with smaller-than-optimal diameter ratios (1.15–1.20) were selected instead of vaned diffusers. The remaining static pressure recovery was achieved through decelerating conical diffusers located downstream of each volute.

Following the preliminary aerothermal design, Computational Fluid Dynamics (CFD) analysis was employed to iteratively refine the three-dimensional blade and volute geometries. The steady-state Reynolds-Averaged Navier–Stokes (RANS) equations were solved using the commercial solver ANSYS CFX 2023-R2. A single-passage computational domain was adopted, with a mixing-plane interface applied between the rotating and stationary components to model the rotor–stator interaction. Turbulence effects were captured using the k–ω SST model.

Table 2: Summary of CFD results of the Compressor Unit for the reference operating point

Parameter	Unit	Stage 1	Stage 2	Stage 3	Stage 4
Rotational Speed	RPM	50 000			
$p_{0.in}$	bar	1.00	1.74	2.54	3.78
$T_{0.in}$	°C	128	220	298	389
Pressure ratio	-	1.76	1.47	1.51	1.33
Flow coefficient (ϕ)	-	0.020	0.020	0.014	0.014
Stage Loading (ψ)	-	0.69	0.75	0.81	0.78
$T_{0.out}$	°C	220	298	389	462
$p_{0.out}$	bar	1.76	2.56	3.82	5.03
$P_{is.cp}$	kW	-25.6			
P_{stage}	kW	-9.4	-8.0	-9.7	-7.8
$\eta_{tt.stage}$	-	74.8%	72.0%	73.7%	72.3%
P_{cp}	kW	-34.9			
Flange to flange isentropic efficeincy	-	67%			

The computational mesh consisted of structured hexahedral elements generated using ANSYS TurboGrid for the impeller and vaneless diffuser, while an unstructured mesh created in ANSYS Meshing was used for the volute. To reduce computational cost, a wall y^+ range of 30–100 was applied in conjunction with the k–ω SST model. A single-passage impeller, diffuser, and a complete volute contains approximately 1.3 million mesh elements. A further refined mesh on the first-stage geometry did not lead to appreciable change in efficiency (0.3%), indicating good grid independence.

The CFD results for the reference operating point are presented in Figure 7, illustrating the total temperature rise across each stage. The results demonstrate that the compressor achieves the target outlet total temperature of approximately 460 °C, and clearly show the contribution of the decelerating conical diffusers to the overall static pressure recovery.

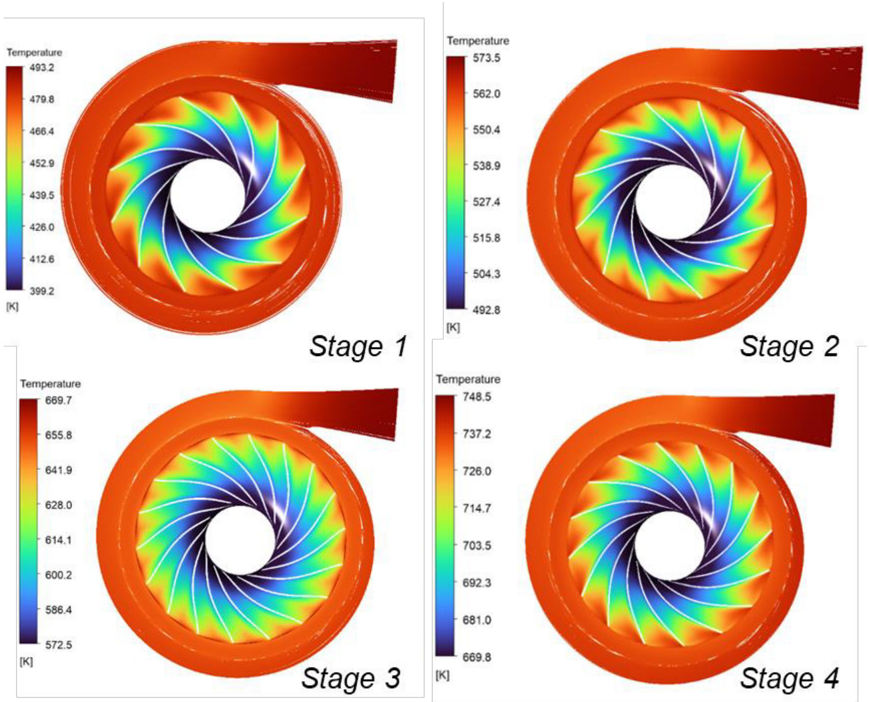

Figure 7: Temperature rise distribution across compressor stages at the reference operating point

In addition to the CFD calculations, thermal calculations were performed to validate the mechanical definition of the motor and its cooling system. A specific cooling circuit was designed to limit the temperature of the bearings and the shaft. Furthermore, ceramic thermal shields were designed.

The compressor operates at outlet air temperatures up to 460 °C, requiring dedicated cooling for both the motor and the rotating assembly. The motor stator is interference-fitted into a laminated iron core housed within an aluminium casing containing a water-cooling circuit. A double-helix channel ensures uniform circumferential temperature distribution by directing coolant in one full revolution and returning in the opposite direction as illustrated in Figure 8 (a).

The water circuit is thermally insulated from the hot gas path using zirconia ceramic shields whose thickness was obtained with 2D Axisymmetric CFD simulations considering the windage losses of the motor, and the thermal flux due to the hot gases from the compressor fluidic path.

The compressor uses spindle-type ball bearings rated up to 100 °C with an air–oil lubrication system, offering higher speed capability and better temperature control than grease lubrication. Oil channels are routed near the water circuit to reduce pre-heating, while centrifugal separator disks remove excess oil. A second oil circuit provides shaft cooling. The same lubricant is sprayed onto the shaft periphery near the centrifugal disk, which simultaneously acts as an oil-ejector and a rotating heat exchanger. This secondary flow rate is higher than the one required for bearing lubrication alone, ensuring additional heat removal from the shaft region.

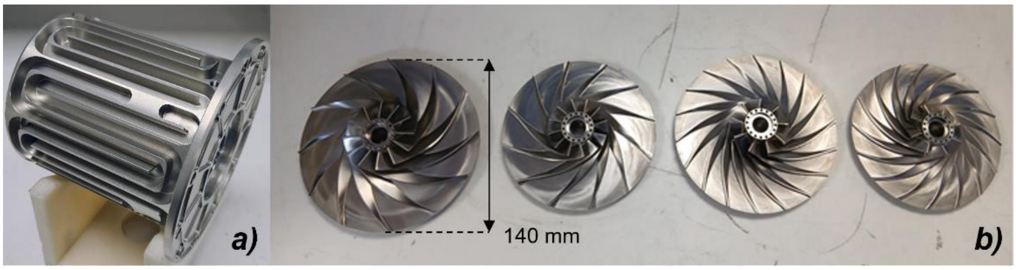

Figure 8: a) Double-helix cooling channel geometry of the motor housing, showing the counterflow water path designed for uniform circumferential temperature distribution. b) Picture of the 4 manufactured runners.

To prevent hot process gas ingress into the motor cavity, a labyrinth seal was implemented between the compressor flow path and the bearing housing. This non-contact sealing minimizes leakage and frictional losses while effectively isolating the cooled mechanical components from the high-temperature gas domain.

Together, the integrated thermal management system, combining active water cooling, air–oil lubrication, ceramic insulation, and labyrinth sealing maintains safe operating temperatures for the bearings and motor. These measures minimize thermal conduction from the hot gas path and ensure the mechanical reliability of the turbomachine under high-temperature operating conditions.

4.2.2. Turbine design

A single-stage, partial-admission supersonic axial turbine of impulse type was selected for the prototype. The turbine is coupled to a permanent magnet synchronous machine (PMSM) operating as a generator, rated at 10 kW and 50,000 rpm. To avoid the very low blade heights associated with full admission which would increase secondary losses, a 50% partial admission configuration was adopted.

The turbine preliminary sizing was performed following Aungier’s methodology [15]. A supersonic nozzle was designed in SolidWorks to meet the throat and exit areas required for the reference operating point:

- Total inlet pressure: 5 bar
- Total inlet temperature: 92 °C
- Mass flow rate: 0.1 kg/s
- Static outlet pressure: 1 bar

CFD analysis performed in ANSYS CFX similar to the Compressor analysis confirmed that, under the reference operating conditions, the required choked mass flow was achieved, as also shown in the Figure 9 (b). Furthermore, the complete stage comprising both the nozzle and rotor achieved a total-to-static isentropic efficiency of approximately 70% with the streamlines illustrated in Figure 9 (a).

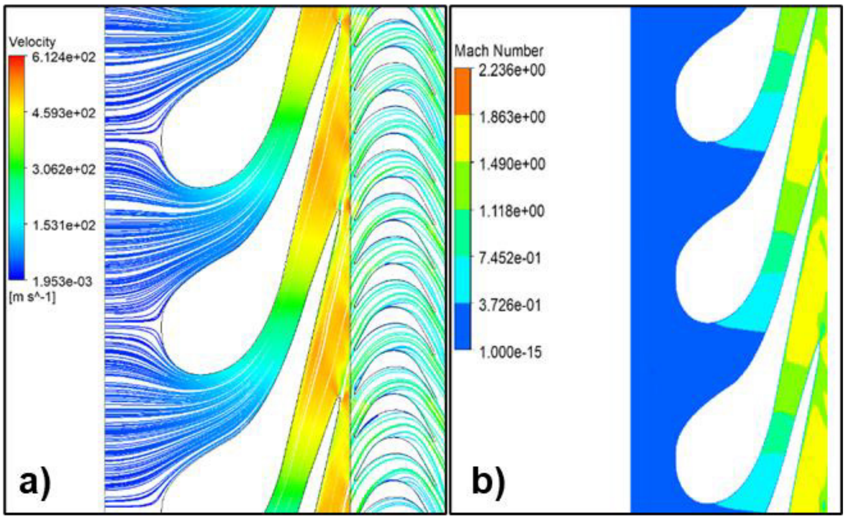

Figure 9: **a)** Velocity streamlines at midspan of the turbine, illustrating the flow behavior through the rotor passage under reference operating conditions. **b)** CFD results showing the Mach-number distribution under reference operating conditions.

Since the rotor bearings were selected under the assumption of negligible axial thrust, the blade angles were optimized to produce an almost isobaric rotor, minimizing axial loading. Finally, because the turbine outlet temperature is below 5 °C, thermal management requirements are minimal. Cooling of the generator is achieved through a water jacket integrated into the aluminium motor–stator casing, maintaining motor temperatures below 60 °C.

In addition to the turbine, which operates under choked flow conditions, an ejector valve was installed in parallel with the turbine to handle off-design operating points. This configuration prevents surge or stall in the compressor by allowing excess mass flow to bypass the turbine when the system flow rate is limited by the choked turbine.

5. Conclusion

This paper has presented work done on a very high-temperature heat pump concept which can heat up fluid up to 430 °C. A numerical study was performed on several case studies involving different strategies for recovering waste heat available at various temperature levels (20 to 150 °C). This study has analysed how the heat-pump architecture and the choice of working fluid influence performance across these scenarios. Several interesting configurations have been identified. The numerical study also highlights the necessity of using an appropriate COP definition to correctly compare different configurations.
To validate these findings, a prototype with a capacity of several tens of kilowatts will be developed. It will be possible to evaluate different architectures and fluid with this prototype. CFD simulations have been carried out by Enogia to design compressors and turbine of the machine. These components will be manufactured by the end of 2025 and machine will be characterized in S1 2026.

Acknowledgements

The authors would like to express their gratitude to Carnot Energies of the Future Institute for funding in the BATCAR project.

References

[1] J.-S. Kim *et al.*, 'Thermal Performance Design and Analysis of Reversed Brayton Cycle Heat Pumps for High-Temperature Heat Supply', *Energies*, vol. 17, no. 12, Jun. 2024, doi: 10.3390/en17122953.
[2] IEA Heat Pump Centre, 'Industrial High-Temperature Heat Pumps. Task 1 – Technologies. Yearly Report 2025.', IEA Heat Pump Centre, Report, 2025.
[3] U. Khan, R. Zevenhoven, L. Stougie, and T.-M. Tveit, 'Life cycle cost analysis (LCCA) of Stirling-cycle-based heat pumps vs. conventional boilers', *Clean. Environ. Syst.*, vol. 8, p. 100105, Mar. 2023, doi: 10.1016/j.cesys.2022.100105.
[4] V. Novotny *et al.*, 'Review of Carnot Battery Technology Commercial Development', *Energies*, vol. 15, no. 2, Jan. 2022, doi: 10.3390/en15020647.
[5] 'electronic library - Authorisation Required'. Accessed: Nov. 17, 2025. [Online]. Available: https://elib.dlr.de/cgi/sfr_auth/krb5login.cgi?loginparams=%2F198466%2F1%2FHPC2023_DLR_Jende_revised.pdf
[6] M. Budt, D. Wolf, R. Span, and J. Yan, 'A review on compressed air energy storage: Basic principles, past milestones and recent developments', *Appl. Energy*, vol. 170, pp. 250–268, May 2016, doi: 10.1016/j.apenergy.2016.02.108.
[7] L. Weisbrodt, 'SUMMARY REPORT ON TECHNICAL EXPERIENCES FROM HIGH-TEMPERATURE HELIUM TURBOMACHEVERY TESTING IN GERMANY'.
[8] A. Caraballo, S. Galán-Casado, Á. Caballero, and S. Serena, 'Molten Salts for Sensible Thermal Energy Storage: A Review and an Energy Performance Analysis', *Energies*, vol. 14, no. 4, p. 1197, Jan. 2021, doi: 10.3390/en14041197.
[9] A. G. Fernández, H. Galleguillos, E. Fuentealba, and F. J. Pérez, 'Thermal characterization of HITEC molten salt for energy storage in solar linear concentrated technology', *J. Therm. Anal. Calorim.*, vol. 122, no. 1, pp. 3–9, Oct. 2015, doi: 10.1007/s10973-015-4715-9.
[10] V. Turek *et al.*, 'Industrial Waste Heat Utilization in the European Union—An Engineering-Centric Review', *Energies*, vol. 17, no. 9, Apr. 2024, doi: 10.3390/en17092084.
[11] *REFPROP*. (2018). NIST, U.S Secretary of Commerce.
[12] 'Accueil', ENOGIA. Accessed: Nov. 17, 2025. [Online]. Available: https://enogia.com/
[13] M. Casey and C. Robinson, *Radial Flow Turbocompressors: Design, Analysis, and Applications*. Cambridge: Cambridge University Press, 2021. doi: 10.1017/9781108241663.
[14] R. H. Aungier, 'Centrifugal Compressor Stage Preliminary Aerodynamic Design and Component Sizing', presented at the ASME 1995 International Gas Turbine and Aeroengine Congress and Exposition, American Society of Mechanical Engineers Digital Collection, Feb. 2015. doi: 10.1115/95-GT-078.
[15] R. H. Aungier, 'AXIAL-FLOW AND RADIAL-INFLOW TURBINE DESIGN AND ANALYSIS'.